Journal of the European Ceramic Society 20 (2000) 403–412

# XRD microstructural analysis of mullites obtained from kaolinite–alumina mixtures

M.A. Sainz [a,*], F.J. Serrano [b], J.M. Amigo [b], J. Bastida [b], A. Caballero [a]

[a] *Instituto de Cerámica y Vidrio, C.S.I.C., 28500 Arganda del Rey, Madrid, Spain*
[b] *Departamento de Geología, Universidad de Valencia (E.G.), 46100 Burjassot, Valencia, Spain*

Received 15 August 1998; received in revised form 10 June 1999; accepted 3 July 1999

**Abstract**

A microstructural study of mullite obtained by the reaction sintering of kaolinite–α–alumina mixtures in the range 1150–1700°C has been performed by using X-ray line profile analyses together with scanning and transmission electron microscopy equipped with microanalysis by energy dispersion (SEM-EDS, TEM-AEM). Two kinds of morphology corresponding to primary (elongated grains) and secondary (equiaxed grains) mullite have been observed. A bimodal crystallite size distribution has been detected through XRD microstructural analysis from 1300°C. The results obtained by this method are compared with SEM/TEM data.


*Keywords:* Grain growth; Mullite; X-ray methods; $Al_2O_3$; Kaolinite

## 1. Introduction

Mullite is a promising material for advanced ceramics applications due to its low thermal expansion, good chemical and thermal stability, very low dielectric constant and because of its high creep resistance.[1,2] Although extensive efforts have been made to synthesize mullite powders[3–5] and to prepare dense sintered bodies, these methods involve very high cost starting materials and powder processing and are consequently not appropriate for large scale production. Cheaper alternative ways of synthesis using such raw materials as kaolinite, kaolinite + alumina or sillimanite have accordingly been a frequent subject of research.[3,6]

Kaolinite ($2SiO_2 \cdot Al_2O_3 \cdot 2H_2O$) is one of the most used starting materials for aluminosilicate-based ceramics, due to its common occurrence and good availability. Natural kaolinite coexists with minor constituents such as mica and quartz. In the present work, the reaction sintering of kaolinite–alumina mixtures[6] has been used in the synthesis of the mullite samples studied. The processing route employed can be explained according to the following reactions:[7]

A. During firing at 1300°C or below, monosized primary mullite crystals were formed only in the kaolinite from metakaolinite decomposition, leaving α-alumina largely inert. At these temperatures the reaction between kaolinite and alumina was limited.

B. At temperatures higher than 1400°C secondary mullite formation takes place by dissolution of alumina into the transitory liquid phase, followed by the precipitation of mullite crystals.

Bimodal mullite crystals indicating secondary mullite nucleation and primary mullite growth were observed by Liu et al[7] in samples fired at 1400°C. The rate of the secondary mullite formation was very slow at $T \leqslant 1555$°C but increased rapidly at $T \geqslant 1595$°C in the presence of a liquid phase. According to Liu et al.,[7] the rapid kinetics of secondary mullite formation, the characteristics of the coexisting glassy phase and the evidence of liquid phase sintering strongly suggest that solution–precipitation via a transitory liquid phase was the major mechanism for secondary mullite formation. Secondary mullite formation via solid state inter-diffusion may occur in parallel, but its contribution to secondary mullite formation can only be regarded as minor.

If the firing temperature is $\geqslant 1595$°C, the rate of reaction is substantially increased not only because of the larger amount of liquid available but also because

* Corresponding author.

0955-2219/00/$ - see front matter 
PII: S0955-2219(99)00183-1

this equilibrium liquid is less rich in silica, and consequently its viscosity diminishes thereby fostering the solution–precipitation process. This sintering mechanism, by a transitory liquid phase, is operative in many ceramic systems provided that the starting materials are not compatible in the solid state.

There are many papers concerning the microstructural features of mullites obtained by different ways including kaolin–alumina reactive sintering,[8,9] but there has been little attempt to use XRD for the microstructural analysis of mullite. McGee et al.[10] and Li et al.[11] give data resulting from the application of the Scherrer equation and more recently Serrano et al.[12] and Sainz et al.[13] show microstructural analysis from a more developed X- ray diffraction profile line analysis.

XRD line broadening is caused by specimen and experimental factors. Within the former, the small size of crystal domains (crystallites) and the lattice strains of the specimen are the two main causes for line broadening, whereas wavelength distribution and geometric instrumental aberrations are the other factors that contribute to line broadening. Size and strain parameters corresponding to the diffracting sample can be determined simultaneously by using several XRD line profile analysis methods. One of these methods is the well-known procedure of Warren and Averbach,[14] which is based on the analysis of the Fourier coefficients. Another method, such as the Voigt function method,[15] is based on a simplified procedure in which the size and strain parameters can be extracted from the precise XRD pattern of a single peak.

In the present work the microstructural studies of the samples obtained by reaction sintering of kaolinite–alumina between 1150 and 1700°C have been performed mainly by XRD line profile analyses and also by SEM/TEM studies. The aim of this paper is to study the microstructural parameters deduced from line profile analysis and to compare these with microstructural features derived from SEM and TEM observations.

## 2. Experimental procedure

### 2.1. Materials and processing

The starting materials were a commercial purity kaolinite (Caobar S.A., Spain) with $d_{50} = 3\,\mu m$, $S_s = 9.2\ m^2/g$ and purity α-alumina (Alcoa-CT 3000 SG, USA) with $d_{50} = 0.5\,\mu m$, $S_s = 8.0\ m^2/g$. The chemical compositions of the starting materials are listed in Table 1. The kaolinite was mixed with the -alumina to give a total composition of 73 wt% $Al_2O_3$.

The processing scheme adopted is the following: the mixed kaolinite–α–alumina powders were first homogenized with isopropyl alcohol in an attritor for 1 h, dried at 60°C followed by 63 μm sieving and isostatic pressing at 200 MPa to form green compacts. Specimens were cut into pellets 10 mm high and 7 mm in diameter and were fired in air at a heating rate of 2°C/min up to 500°C, followed by 5°C/min heating to different temperatures (1150–1700°C) where they were soaked for 4 h and rapidly cooled. The results were studied by XRD, SEM-EDS and TEM-AEM.

Table 1
Chemical composition of starting materials (wt%)

| | Kaolinite (Caobar S.A.) | α-alumina (Alcoa-CT) |
|---|---|---|
| $SiO_2$ | 48.40 | 0.08 |
| $Al_2O_3$ | 37.00 | 99.20 |
| $Fe_2O_3$ | 0.25 | 0.03 |
| $TiO_2$ | 0.002 | – |
| MgO | 0.05 | 0.10 |
| CaO | 0.31 | – |
| $Na_2O$ | 0.13 | 0.12 |
| $K_2O$ | 0.46 | – |
| L.O.I. | 13.4 | 0.5 |

### 2.2. Microscopical observation

Microscopical observations have been performed on samples fired between 1500 and 1700°C by SEM-EDS and TEM-AEM. The samples were cut into disks and finely polished using 6, 3 and 1 μm diamond suspension. Then were also thermal etches between 1300 and 1500°C for 30 min and chemical etches with a 10% HF solution for 30 s. The SEM-EDS included a digitalized microscope (model DSM 950, Karl Zeiss, Thornwood, NY) and a spectrophotometer series ZII, Tracor Norther, Middleton, WI.

The analytical electron microscopy (AEM) was carried out on specimens prepared by ionic beam thinning in an Elatan machine avoiding damage of the analysed samples. The TEM was conducted with a Philips 400T electron microscope equipped with a Kevex 8000 Analyst EDS system.

The grain size of mullite was measured on the SEM/TEM micrographs by Image Analysis methods (Imagist II system, PGT equipment).

### 2.3. Methods of line profile analysis

Two methods of XRD line profile analysis have been used to obtain information about microstructural characteristics of the diffracting sample. The parameter most used to estimate the widening is $2w$ (full width at half the maximum intensity). Size and strain parameters corresponding to the diffracting sample can be determined simultaneously by using several XRD line profile analysis methods.

#### 2.3.1. Voigt function[15]

This method is a simplified procedure that can extract size and strain parameters from the precise XRD pattern

of a single peak. The diffraction profile is assumed to be Voigtian (convolution of Cauchy and Gaussian profiles) because it has been proved[16] that the real diffraction profiles are well adjusted to the Voigt function. The Cauchy and Gaussian components of the measured profiles are related to the microstructural parameters (size and strain) of the diffracting sample. The formula used for the size parameter is:

$$< D_v >= \frac{\lambda}{\beta_{c_f} \cos\theta} \quad (1)$$

$< D_v >$ corresponds to the crystallite size, $\beta_{Cf}$ is the integral breadth of the cauchyan component of the real profile expressed in rad, λ is the wavelength used, and $\theta$ the Bragg angle for the $\alpha_1$ component.

On the other hand, the strain parameter is given by:

$$\mathbf{e} = \frac{\beta_{Gf}}{4 \tan\theta} \quad (2)$$

where $\beta_{Gf}$ is the integral breadth of the gaussian component of the real profile expressed in rad and $\theta$ is the Bragg angle for the $\alpha_1$ component.

#### 2.3.2. Warren–Averbach[14]

This method is based on the analysis of the coefficients of the Fourier series that describe the XRD profiles, and it is usually considered to be an accurate tool for the microstructural characterization of crystalline samples. This method requires at least two orders of the same reflection corresponding to the studied sample in order to separate the contributions to the peak broadening produced by domain size and strains.

The input data for the Warren–Averbach method (by means the Win-Crysize program, supplied by Siemens) are the XRD line profiles obtained for the two selected peaks (110 and 220 in this case) of sample and standard. On the other hand, the outputs of this program are: a header, listing peak positions and Miller indices of the used peaks, a list of microstrains as a function of distance $L$ in 1 nm intervals, the average column length (the average crystallite size $\langle D_s \rangle$), the most frequent column length (maximum of relative frequency distribution), the width of the relative frequency distribution, the relative frequency of column lengths in 1 nm intervals.

The size parameter obtained is $\langle D_s \rangle$ which represents an "effective" size, since it is related to the broadening from the domain size, but also from faulting and twinning. The usual parameter of strain is RMS (root mean square strain) for $L = 50$ Å. This is a parameter indicative of the microstrain $(\Delta L/L)$ associated with length $L$, considering all the columns of crystallites of the diffracting sample. Both $\langle D_s \rangle$ and RMS for $L = 50$ Å are the most used microstructural parameters, but the results concerning the frequencies of column lengths expressed as the rate between $N_L$ (number of columns with column length $L$) and the overall number of columns in the sample could be interesting as in the case of this paper.

### 2.4. X-ray diffraction measurements

For XRD analyses a small quantity of fired material at different temperatures was ground with a tungsten carbide mortar and pestle to obtain finely powdered samples. The powders obtained were identified by XRD powder methods and indexed considering the mullite spatial group *Pbam* and $a = 7.545$ Å, $b = 7.689$ Å and $c = 2.884$ Å.

X-ray measurements were made using a conventional Siemens D-500 diffractometer operating at 50 Kv and 30 mA, interfaced to an IBM-PC running the Socabim PC software package DIFFRAC-AT. Ni filtered Cu$K_\alpha$ radiation was used.

X-ray diffraction powder patterns over the range 2–62° ($2\theta$) were performed for crystalline phase identification. Measurements of the intensities of the 210 mullite reflection (step width of 0.025° $2\theta$ and measurement times of 3 s) were done in order to evaluate the mullite content at different firing temperatures.

The 110, 120, 210, 001, 220, 111 and 121 reflections of mullite were selected for line profile analysis performed on slow recordings of powder samples. The experimental conditions for data collection were as follows: step width of 0.025° 2 and measurement times of 1.5 and 4 s was used in fast recordings for mineralogical identification. XRD patterns obtained for line profile analysis were recorded with a step width of 0.005° $2\theta$ and with variable measurement time (depending on the intensity of the peak) ranging from 25 to 36 s, in XRD patterns for line profile analysis.

Standard profiles, needed for the evaluation of instrumental line broadening in selected X-ray patterns, were obtained from purified mullite formed by firing at 1700°C/2 h and after removal of a vitreous phase by acid leaching technique.[17]

The line profile analyses of selected reflections of mullite were performed by using the program FIT, available in the software package DIFFRAC-AT. The experimental profiles were fitted to analytic functions (pseudo-Voigt and split-Pearson VII) after subtraction of an adjusted linear background and taking into account the effect of the Cu$K\alpha_2$ component on the experimental profile. The parameter used to estimate the goodness of the fit was $R_{pf}$ ($R$: reliability, pf: profile fitting) defined as:

$$R_{pf} = \left[\frac{\Sigma(I_{obs} - I_{calc})^2}{\Sigma I_{obs}^2}\right]^{0.5} \cdot 100 \quad (3)$$

where $I_{obs}$ and $I_{calc}$ are the observed and calculated intensity,[18] respectively.

The initial data used for the application of the Voigt function and the Warren–Averbach methods were obtained from the profiles fitted to analytical functions. The Warren–Averbach method has been applied by using the program WIN-CRYSIZE, supplied by Siemens. Two orders of the same reflection are needed for the application of this method, so we have used the 110 and 220 reflections in order to evaluate the crystallite size in the [110] direction; this has been possible because these reflections are intense and relatively isolated (no overlapping with other peaks). For the other directions, there are not two orders of reflection corresponding to intense peaks without interference with other reflections so the Voigt function method was used since it requires only one peak for the microstructural analysis.

## 3. Results and discussion

TEM microscopy was used to provide information on the distribution and size of mullite crystallites at lower temperatures. Fig. 1 shows that the mullite crystals formed after 4 h firing at 1150°C were typically 200–300 Å in width and generally had a large aspect ratio. Fig. 2 shows slightly larger mullite crystals, 300–500 Å, were formed in the specimen fired at 1300°C for 4 h. These mullite crystals had a narrow size distribution and were aggregated in the plate-like metakaolinite base, leaving the α-alumina grains largely inert. These results indicate that at 1300°C the reaction between kaolinite and α-alumina was limited and the primary mullite crystals were formed only in kaolinite. After firing at 1400°C/4 h, the sample shows the existence of large mullite crystals (≫1000 Å) with a higher aspect ratio corresponding to primary mullite grown in a glassy matrix (Fig. 3) and smaller secondary mullite crystals (≈500 Å) nucleated from the transitory liquid by the dissolution of alumina.

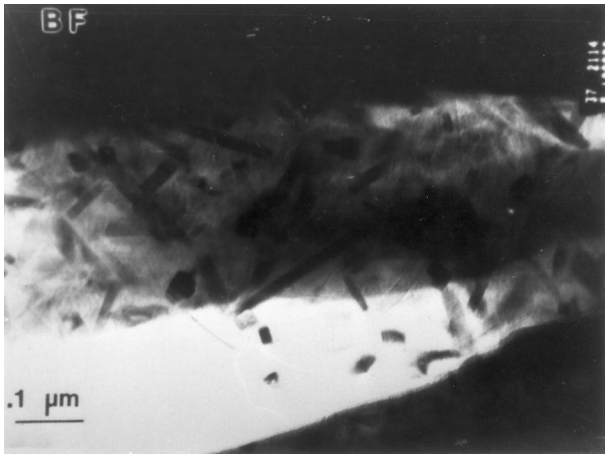


Fig. 1. TEM micrograph of specimen fired at 1150°C shows needle-like primary mullite crystals formed in kaolinite.

Also at this temperature the residual alumina was appreciably less as was also evidenced by XRD studied.

The SEM-EDS results revealed that after firing at 1500°C/4 h the samples showed a bimodal morphology. Fig. 4 shows that the grain morphology appeared to be a mixture of equiaxed secondary mullite crystals and lath-like primary mullite crystals grown, in the same environment, with a larger aspect ratio. The smaller mullite crystals were the secondary mullite nucleated from the transitory liquid phase and the dissolution of alumina in this liquid phase.[7] The larger mullite crystals with a higher aspect ratio correspond to the primary mullite nucleated in kaolinite and grown in the firing. The average sizes of the mullite grains were: $0.3 \pm 0.2$ μm for secondary and $1.2 \pm 0.2$ μm long and $0.4 \pm 0.2$ μm wide for primary mullite.

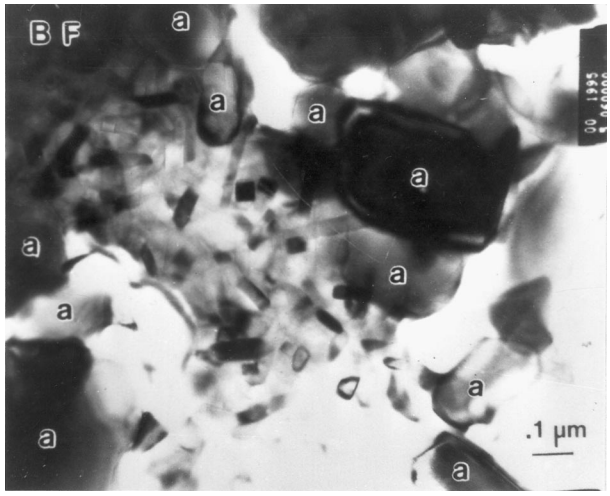


Fig. 2. TEM bright field images of sample treated at 1300°C, showing growth crystallites of primary mullite and also α-alumina grains (a: α-alumina).

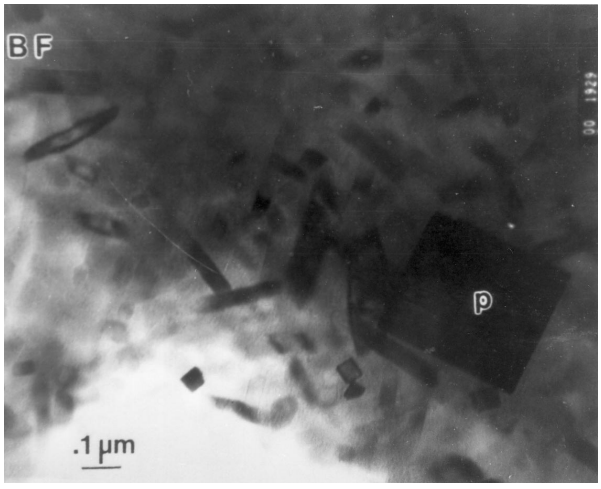


Fig. 3. TEM micrograph of sample firing at 1400°C, showing smaller secondary mullite crystals and larger primary mullite crystals (p: primary mullite).

At 1600°C (Fig. 5) bimodal morphology was again observed. In this case the larger mullite crystals were well defined. The average sizes of the mullite grains were: $0.7 \pm 0.2\,\mu m$ for secondary and $2.4 \pm 0.5\,\mu m$ long and $0.9 \pm 0.2\,\mu m$ wide for primary mullite.

At 1650°C (Fig. 6) bimodal morphology is clearly present in the sample. The size of the primary mullite crystals showed a slightly increase with respect to the sample treated at 1600°C. The average sizes of the mullite grains were: $0.8 \pm 0.2\,\mu m$ for secondary and $3.2 \pm 0.5\,\mu m$ long and $0.9 \pm 0.2\,\mu m$ wide for primary mullite. According to the $Al_2O_3$–$SiO_2$[26] system at temperatures higher than 1600°C the process of dissolution of mullite in the permanent liquid phase starts, and consequently an increase in the size of the mullite crystals is expected.

A good example showing the bimodal morphology of mullite crystals, both embedded in a glassy matrix, can be found in the specimen fired at 1650°C by TEM microscopy (Fig. 7).

At 1700°C, by SEM microscopy it was possible to observe (Fig. 8) that the mullite crystals were bimodal in size with the smaller ones in the micron range ($1.2 \pm 0.2\,\mu m$ secondary mullite) and very large grains often with a very distinctive lath-like shape despite the fact that they had substantially grown in size ($5.3 \pm 0.5\,\mu m$ long and $1.7 \pm 0.2\,\mu m$ wide for primary mullite). This evolution is typical of mullite at high temperature in the presence of a liquid phase.[2,19]

A quantitative microstructural analysis of mullite grains size was carried out on polished sections of samples

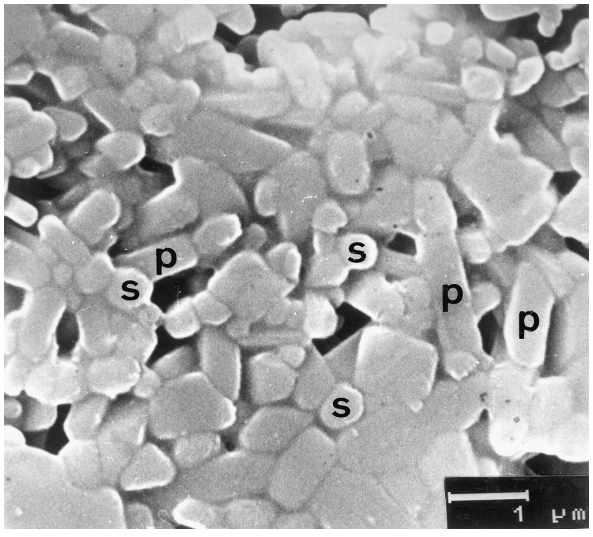


Fig. 4. SEM micrograph of kaolinite-alumina mixture treated at 1500°C showing two morphologies of mullite grains (p: primary mullite, s: secondary mullite).

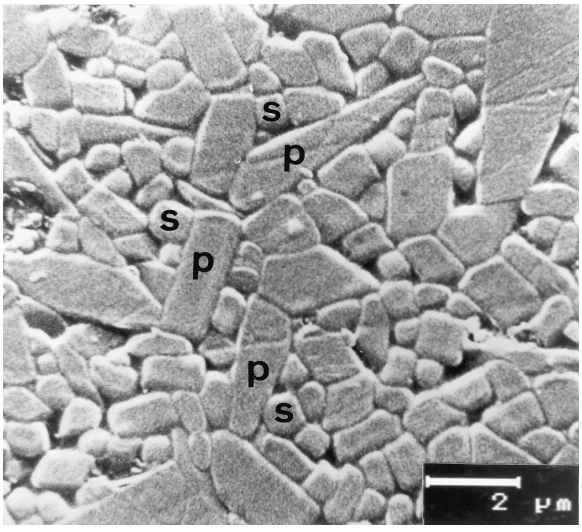


Fig. 6. SEM micrograph of sample fired at 1650°C (p: primary mullite, s: secondary mullite).

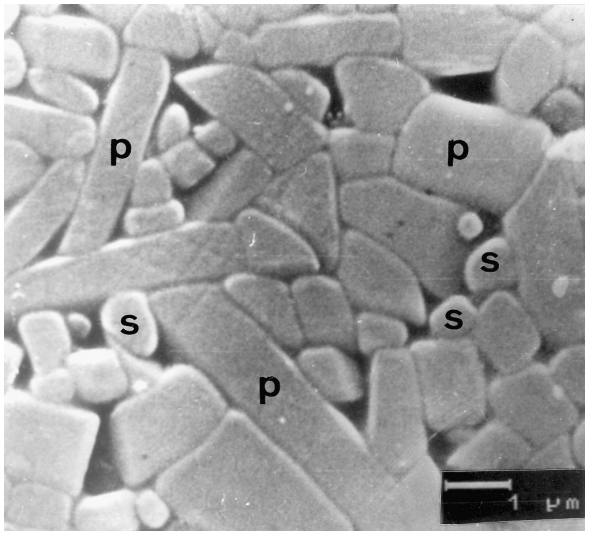


Fig. 5. SEM micrograph of the sample fired at 1600°C, bimodal morphology was observed (p: primary mullite, s: secondary mullite).

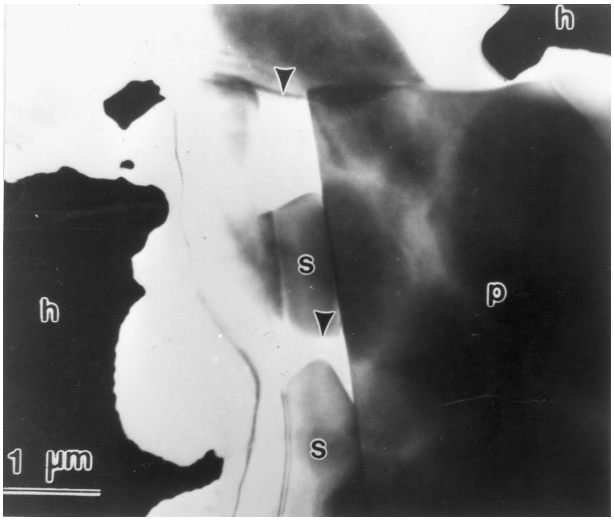


Fig. 7. TEM micrograph of kaolinite-alumina sample showing the bimodal morphology of mullite crystals obtained after fired at 1650°C (s: secondary mullite, p: primary mullite, h: hole).

treated between 1500 and 1700°C. The grain size of mullite was measured on SEM micrograph by Image Analysis methods. Fig. 9 shows the relative frequency versus average grain size distribution as a function of the temperature. The data were obtained considering the length to primary mullite and the equivalent average diameter to secondary mullite. The results obtained support strongly the bimodal feature above 1500°C. On the other hand, both maximal frequencies of average grain size are shifted to greater values, reflecting grain size growth of both mullites when the temperature is increased. This shift being greater for the greater sizes indicated a greater growth rate for primary mullite while secondary mullite only shows a slight growth. The greater growth of primary mulite with respect to secondary in the presence of permanent liquid phase can be justified due to growth in the natural direction of elongation in crystals as a consequence of the lower interfacial energies of crystal faces parallel to the *c* axis direction[20] (coincident with the elongation direction of crystals).

The chemical composition of many mullite grains was measured in different points of the sample by TEM-AEM. Table 2 shows the characteristic chemical composition of different mullite grains for the sample sintered at 1650°C (Fig. 7). The compositions of primary and secondary mullites vary significantly as expected from the $Al_2O_3$–$SiO_2$[26] system, because primary mullite has composition close to point 1 and secondary mullite is richer in alumina content close to point 2 (Fig. 10).

Moreover microprobe analysis of the glassy phase obtained by TEM-AEM (Table 2) shows a great variance at lower temperatures, up to 1500°C (glass formation related to impurities), although for higher temperatures there is little variance (eutectic silica–mullite in the $Al_2O_3$–$SiO_2$ system). The existence of this eutectic liquid, at temperatures around 1595°C, will enhance the formation of secondary mullite.[6]

Fig. 11 shows the X-ray diffraction pattern of the mullite standard (mullite free of vitreous phase by acid leaching technique[17]). Fig. 12 shows the profile evolution of the 001, 220 and 111 reflections of mullite, obtained from slow XRD patterns of samples fired at the range 1550–1650°C, used for the Voigt function methods.

The XRD line profile analysis performed on the mullite samples obtained by reaction sintering of kaolinite–alumina mixtures in the range 1150–1650°C is summarized in Table 3. On fired samples, the mullite crystallinity was estimated from line profile analysis of the selected reflections of mullite. From Table 3, which shows the parameters of the studied profile lines, it is possible to observe that the sample E presents the lowest values of the parameter 2*w* (width peak at half the maximum intensity) for all mullite reflections considered

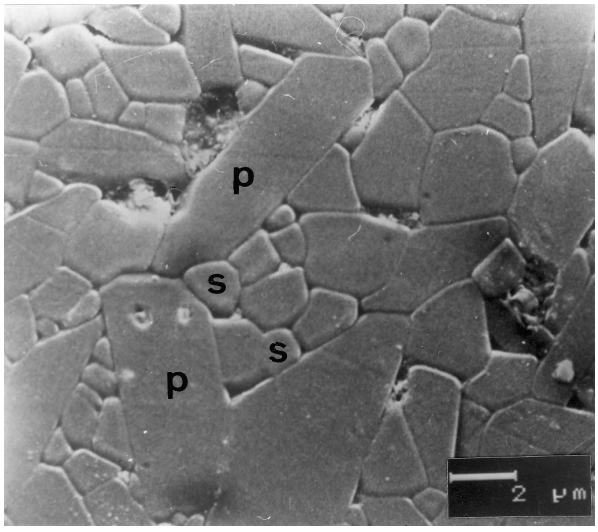


Fig. 8. SEM micrograph of sample fired at 1700°C, The thermal treatment produced grow of primary and secondary mullite grains (p: primary mullite, s: secondary mullite).

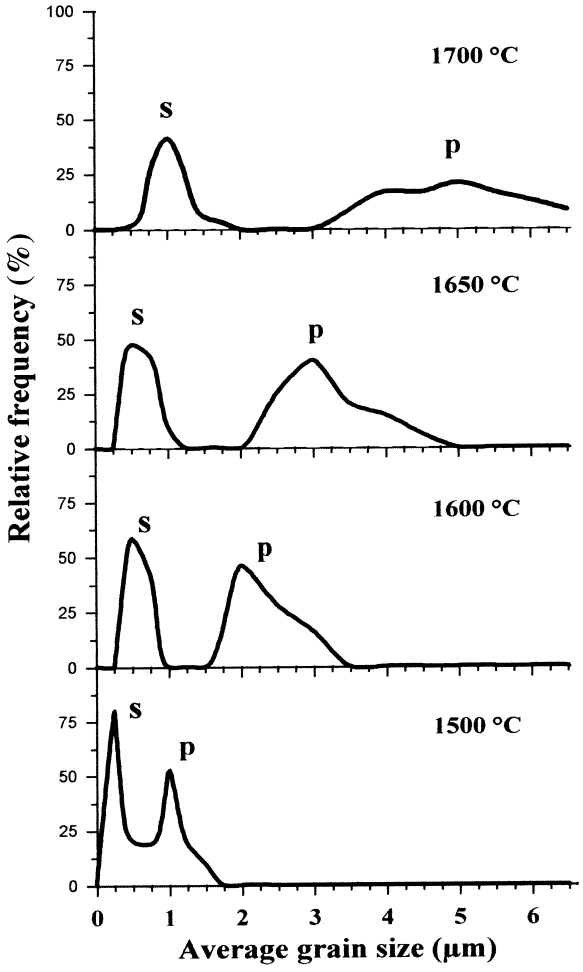


Fig. 9. Relative frequency versus average grain size distribution as a function of the temperature (s: secondary mullite, p: primary mullite).

Table 2
Compsoition of glassy phase from samples sintered at 1500–1600°C/4 h and microchemical composition of mullite grains at 1650°C obtained by TEM-AEM(impurities excluded)

| | wt% $Al_2O_3$ | wt% $SiO_2$ |
|---|---|---|
| *Composition of glassy phase* | | |
| 1500°C | 48.8 | 51.2 |
| | 25.2 | 74.8 |
| | 36.7 | 63.3 |
| 1600°C | 13.0 | 87.0 |
| | 14.4 | 85.6 |
| | 15.4 | 84.6 |
| *Composition of mullite sintered at 1650°C/4 h* | | |
| Primary mullite | 72.2 | 27.8 |
| | 72.0 | 28.0 |
| | 71.7 | 28.3 |
| Secondary mullite | 73.4 | 26.6 |
| | 73.7 | 26.3 |
| | 74.1 | 25.9 |

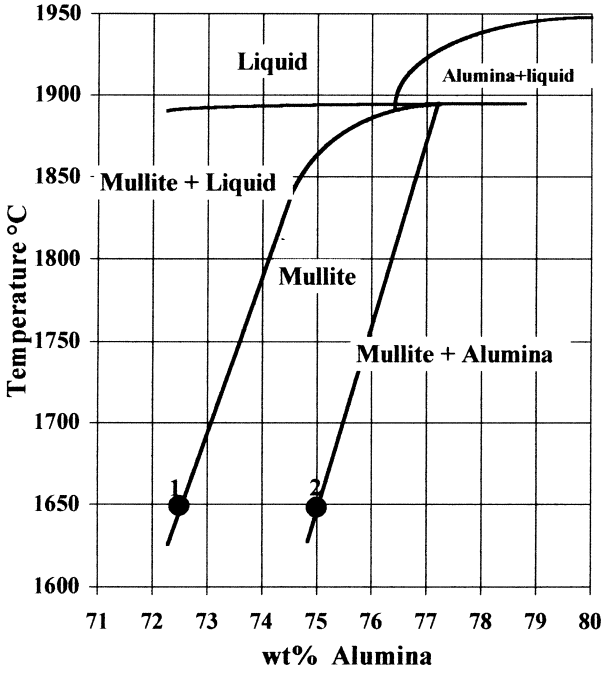


Fig. 10. Expanded area in the $Al_2O_3$–$SiO_2$ system.[26]

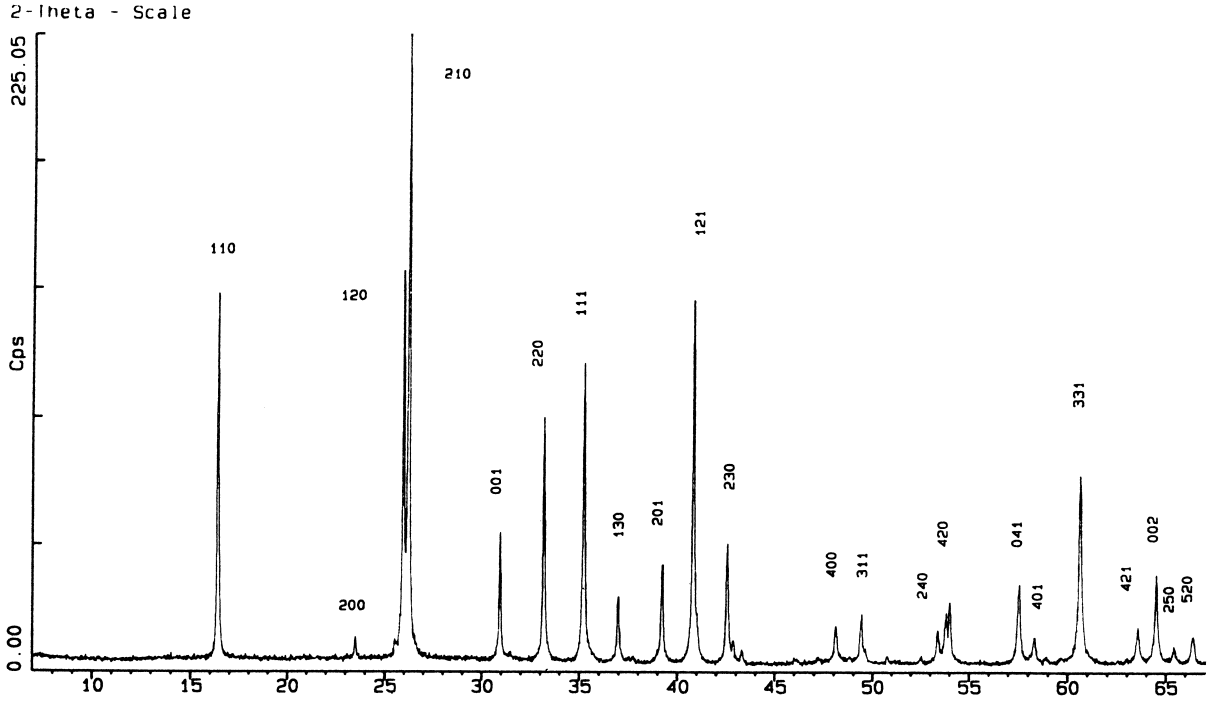


Fig. 11. X-ray diffraction pattern of the standard mullite.

in the analysis. From Table 3 also can be deduced that the sample treated at 1600°C shows the better crystallinity.

Table 4 shows the microstructural parameters obtained by both methods (Warren–Averbach and Voigt function method) from the different analyzed profile lines. The Voigt function method was used to compare the crystallite growth in several crystallographic directions, since it requires only one reflection, although the obtained data are not so accurate as those obtained by the Warren–Averbach procedure. The single line analysis shows an increase of effective crystallite size up to 1600°C along [110], and up to 1400°C along [001], and low and similar values of the strain parameter **e**, except for 1150°C. The more accurate

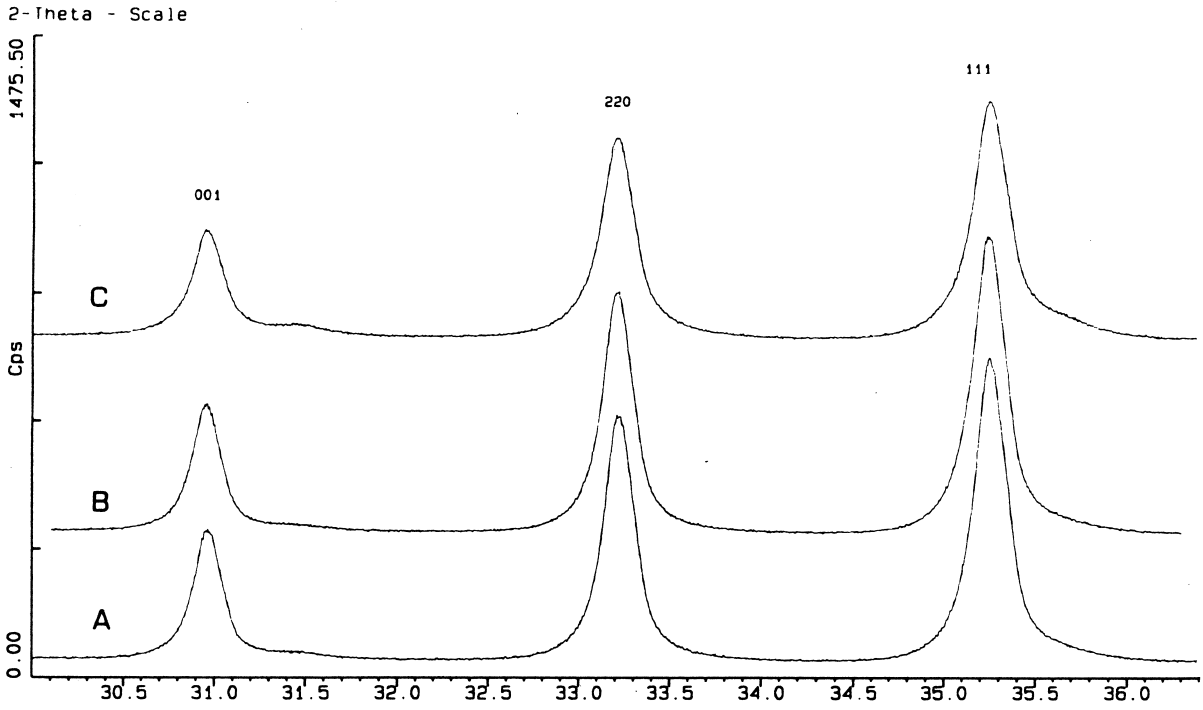


Fig. 12. Some profiles used for XRD line broadening analysis. A, B, C corresponds to mullite treated at 1550, 1600 and 1650°C, respectively.

Table 3
Parameters obtained by using the fitting procedure of XRD peaks performed previously to the microstructural analysis

| Mullite samples (firing temperature) | *hkl* | | | | | | | | |
|---|---|---|---|---|---|---|---|---|---|
| | 110 | | | 001 | | | 220 | | |
| | $R_{pf}$(%) | $2\theta_{obs}$(°) | $2\omega$(°) | $R_{pf}$(%) | $2\theta_{obs}$(°) | $2\omega$(°) | $R_{pf}$(%) | $2\theta_{obs}$(°) | $2\omega$(°) |
| A (1150°C) | 2.79 | 16.428 | 0.3842 | 3.38 | 30.981 | 0.2149 | 3.38 | 33.227 | 0.3860 |
| B (1300°C) | 4.27 | 16.424 | 0.2721 | 3.77 | 30.994 | 0.1995 | 3.77 | 33.233 | 0.2736 |
| C (1400°C) | 6.17 | 16.483 | 0.1940 | 4.55 | 31.027 | 0.1682 | 4.55 | 33.289 | 0.1796 |
| D (1550°C) | 8.77 | 16.353 | 0.1791 | 5.91 | 30.940 | 0.1554 | 4.58 | 33.194 | 0.1698 |
| E (1600°C) | 10.61 | 16.216 | 0.1618 | 5.44 | 30.930 | 0.1559 | 4.31 | 33.187 | 0.1692 |
| F (1650°C) | 9.96 | 16.279 | 0.1807 | 5.46 | 30.933 | 0.1842 | 5.13 | 33.182 | 0.1993 |

data from the Warren–Averbach method, show an increase of effective crystallite size along [110] and without strain (RMS = 0 for A and B) or with low values (in the range of the values in refractory oxides observed by Lewis et al.[21]) but increasing from 1400 to 1600°C. This slight increasing of strain parameters can be related with an increasing number of dislocations; whereas variations in the size parameters can be related to the complex morphological evolution of crystallites. Distribution of crystallite sizes obtained by this method can be considered quite realistic, because there is no strain or very little; it is interesting to observe the existence of two relative maxima which are more evident at temperatures from 1300 to 1550°C (Fig. 13). At higher temperatures the apparent crystallite sizes are large and the XRD microstructural analysis becomes difficult (there is little broadening of the peak compared with the standard peak). Taking into account this effect the results obtained at 1650°C were not considered.

In Table 4 it was also possible to observe that the $\langle D_v \rangle$ values were found to be higher than $\langle D_s \rangle$ because these parameters have different significance.[22] On the other hand the microstrain parameter **e**, which indicates lattice distortion, was observed to decrease in the sample obtained at the higher temperatures.

XRD microstructural data analysis for the direction of least growth, which is [110] according to morphological and structural considerations,[13,23] makes it possible to evaluate the crystallite growth evolution. In the present case, the observed bimodal distribution of crystallite size reveals the relationship between dimensions of crystals (grains) and the XRD effective size of crystallites. Nevertheless each distribution of crystallite size, showing clearly two relative maximal frequencies at

Table 4
Microstructural parameters of mullites evaluated by XRD line broadening analysis and corresponding to samples obtained by reaction sintering of kaolinite–alumina mixtures in the range 1150–1650°C

| Mullite samples (firing temperatures) | *hkl*:110 | | *hkl*:001 | |
|---|---|---|---|---|
| | $\langle D_v \rangle$(Å) | e×10² | $\langle D_v \rangle$(Å) | e×10² |
| *Single line analysis (Voigt function)* | | | | |
| A (1150°C) | 303 | 0.655 | 371 | – |
| B (1300°C) | 374 | 0.288 | 315 | – |
| C (1400°C) | 935 | 0.266 | 1416 | 0.153 |
| D (1550°C) | 1277 | 0.255 | 1290 | 0.117 |
| E (1600°C) | 1651 | 0.208 | 1259 | 0.116 |
| F (1650°C) | 1263 | 0.262 | 887 | 0.149 |
| Mullite samples (firing temperature) | hkl: 110–220 | | | |
| | $\langle D_S \rangle$(Å) | | | RMS×10² |
| *Multiple-line analysis(Warren–Averbach)* | | | | |
| A (1150°C) | 231 | | | 0 |
| B (1300°C) | 372 | | | 0 |
| C (1400°C) | 789 | | | 0.146 |
| D (1550°C) | 995 | | | 0.191 |
| E (1600°C) | 1319 | | | 0.208 |
| F(1650°C) | 1109 | | | 0.244 |

temperatures $\geqslant$1300°C, suggest the existence of two superimposed processes of formation of primary and secondary mullite with different composition and different morphological expression.[24]

This bimodality of grain size distribution has been observed particularly for mullite from kaolinite–alumina[7,25] at temperatures $\geqslant$1400°C by SEM/TEM studies. In the present work this bimodality was study by XRD, TEM and SEM. The evolution of crystallite size distributions with increasing temperatures were obtained by XRD (Fig. 13) which, between 1150 and 1300°C, shows a narrow crystallite size distribution which was attributed to the primary mullite formed mainly by solid state process. At temperatures above 1300°C (Fig. 13) shows that two maximal frequencies are clearly observed, corresponding to secondary mullite nucleation and primary mullite growth. Both maximal frequencies of crystallite size are shifted to greater values reflecting crystallite growth. By Image Analysis methods on SEM micrograph the bimodality has been also studied (Fig. 9), and it has been clearly evidenced that at temperatures above 1600°C the growth of primary and secondary mullite is enhanced and controlled by the presence of permanent liquid phase (Fig. 10).

In a previous work, this method has been applied by Sainz et al.[13] to mullite obtained by thermal transformation of kyanite, with two different morphologies as a function of temperature. In that work it was possible to correlate mullite crystallite size obtained by XRD-line profile with the grain growth of mullite observed by SEM. In the present work it was possible to observe, by XRD-line profile, the simultaneous presence of two mullite morphologies and to determine the evolution of crystallite size for both types of mullite at temperatures from 1300 to 1550°C, corresponding to primary and secondary mullite.

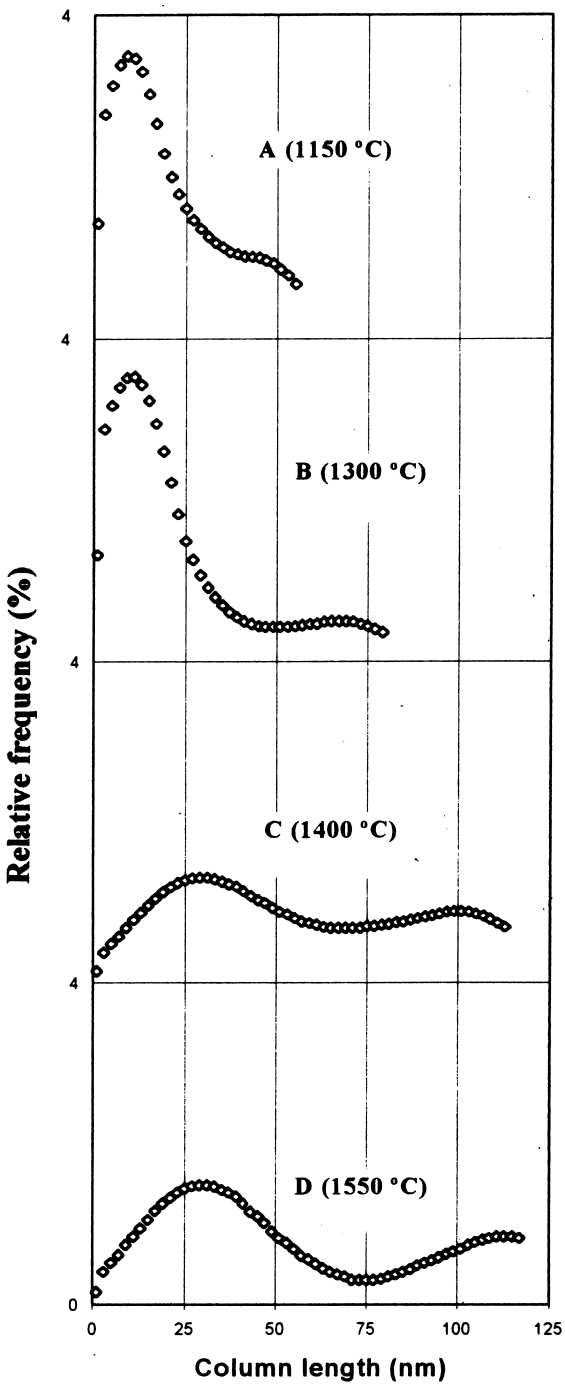


Fig. 13. Crystallite size distribution obtained from XRD line broadening analysis.

## 4. Conclusion

- By X-ray line profile analyses it was possible to observe, between 1300 and 1550°C, the simultaneous presence of two mullite morphologies and the evolution of crystallite size in both mullite morphologies.
- XRD microstructural studies established that bimodal mullite crystals corresponding to secondary mullite nucleation and primary mullite growth were clearly observed at 1300°C, a temperature 100°C lower than that previously determined by TEM studies carried out in mullites also obtained from kaolinite–$\alpha$-alumina mixtures.
- XRD studies showed that, in the temperature range 1300–1550°C, both maximal frequencies of crystallite size are shifted to greater values, reflecting crystallite growth.
- At temperatures higher than 1550°C SEM studies showed that primary and secondary mullite grow simultaneously and that substantial growth in size is observed at 1700°C. This evolution is typical for mullite grown at high temperature in the presence of a permanent liquid phase.

## Acknowledgement

This work was supported by C.I.C.Y.T., Spain under contract No. MAT.97-D728.

## References

1. Aksay, I. A., Dabbs, D. M. and Sarikaya, M., Mullite for structural, electronic, and optical applications. *J. Am. Ceram. Soc.*, 1991, **74**(10), 2343–2358.
2. Schneider, H., Okada, K. and Pask, J. A., Mullite and Mullite Ceramics. John Wiley and Sons, Chichester, UK, 1994, pp. 1–251.
3. Sacks, M. D. and Lee, H.-W., A review of powder preparation methods and densification procedures for fabricating high density mullite. In *Ceramic Transaction, Vol. 6, Mullite and Mullite Matrix Composites*, ed. S. Somiya R. F. Davis and J. A. Pask. American Ceramic Society, Westerville, OH, 1990, pp. 167–207.
4. Okada, K., Otsuka, N. and Somiya, S., Review of mullite synthesis routes in Japan. *Ceram. Bull.*, 1991, **70**(10), 1633–1640.
5. Ghate, B. B., Hasselman, D. P. H. and Spriggs, R. M., Synthesis and characterization of high purity, fine grained mullite. *Am. Ceram. Soc. Bull.*, 1973, **52**(9), 670–728.
6. Liu, K. C., Thomas, G., Caballero, A., Moya, J. S. and De Aza, S., Microstructure and microanalysis of mullite processed by reaction sintering of kaolin–alumina mixtures. *Ceramics Today — Tomorrow's Ceramics, Materials Science Monographs*, 1991, **66A**, 177–186.
7. Liu, K. C., Thomas, G., Caballero, A., Moya, J. S. and de Aza, S., Mullite formation in kaolinite–$\alpha$–alumina. *Acta Metall. Mater.*, 1994, **42**(2), 489–495.
8. Davis, R. F. and Pask, J. A., Diffusion and reaction studies in the system $Al_2O_3$–$SiO_2$. *J. Am. Ceram. Soc.*, 1972, **55**, 525–531.
9. Obadia, S. and Broussaud, D., Microstructural development in $Al_2O_3$–$SiO_2$ sintered ceramics for high temperature application. *Sci. Ceram.*, 1988, **14**, 431–436.
10. McGee, T. D. and Wirkus, C. D., Mullitization of alumino-silicate gels. *Bull. Am. Ceram. Soc.*, 1972, **51**(7), 577–581.
11. Li, D. X. and Thomson, W. J., Mullite formation kinetics of a single-phase gel. *J. Am. Ceram. Soc.*, 1990, **73**(4), 964–969.
12. Serrano, F. J., Bastida, J., Amigo, J. M. and Sanz, A., XRD line broadening studies on mullite. *Cryst. Res. Technolo.*, 1996, **31**(8), 1085–1093.
13. Sainz, M. A., Serrano, F. J., Bastida, J. and Caballero, A., Microstructural evolution and growth of crystallite size of mullite during thermal transformation of kyanite. *J. Eur. Ceram. Soc.*, 1997, **17**, 1277–1284.
14. Warren, B. E. and Averbach, B. C., The effect of cold-work distorsion on X-ray patterns. *J. Appl. Phys.*, 1950, **21**, 595–599.
15. Delhez, R., De Keijser, Th.H. and Mittemeijer, E. J., Determination of crystalline size and lattice distorsions through X-ray diffraction line profile analysis. *Fresenius Z. Anal. Chem.*, 1982, **1-16**, 312.
16. Langford, J. I., A rapid method for analysing breadths of diffraction and spectral lines using the Voigt function. *J. Appl. Cryst.*, 1978, **11**, 10–14.
17. Wancheng, Z., Litong, Z. and Hengzhi, F., Modification of the hydrofluoric acid leaching technique: part I. *J. Am. Ceram. Soc.*, 1988, **71**(5), 395–398.
18. Will, G., Parrish, W. and Huang, T. C., Crystal-structure refinement by profile fitting and least-squares analysis of powder diffractometer data. *J. Appl. Cryst.*, 1983, **16**, 611–622.
19. Saruhan, B., Voss, U. and Schneider, H., Solid solution range of mullite up to 1800 and microstructural development of ceramics. *Journal of Materials Science*, 1994, **29**(12), 3261–3268.
20. Johnson, S. M. and Pask, J. A., Role of impurities on formation of mullite from kaolinite and $Al_2O_3$–$SiO_2$ mixtures. *Am. Ceram. Soc. Bull.*, 1982, **61**(8), 838–842.
21. Lewis, D. and Lindley, M. W., An X-ray line broadening study of the introduction and removal of strain in some refractory oxides. *J. Amer. Ceram Soc.*, 1965, **47**(12), 652–653.
22. Balzar, D., Profile fitting of X-ray diffraction lines and Fourier analysis of broadening. *J. Appl. Cryst.*, 1992, **25**, 559–570.
23. Serrano, F.J., Análisis microestructural de mullitas por difracción de rayos X. Ph.D. thesis, Universidad Valencia, Burjassot, Valencia, Spain, 1995.
24. Lifshitz, I. M. and Slyozou, V. V., The kinetics of precipitation from supersaturated solid solutions. *J. Phys. Chem. Solids*, 1965, **19**, 35–50.
25. Rezaie, H. R., Rainforth, W. M. and Lee, W. E., Mullite evolution in ceramics derived from kaolinite, kaolinite with added $\alpha$-alumina, and sol–gel precursors. *Brit. Ceram. Trans.*, 1997, **96**(5), 181–187.
26. Klug, F. J., Prochazka, S. and Doremus, R. H., Alumina–silica phase diagram in the mullite region. *J. Am. Ceram. Soc.*, 1987, **70**(10), 750–759.